Supporting Information:

Quantifying the ultra-slow desorption kinetics of
2,6-naphthalenedicarboxylic acid monolayers at
liquid-solid interfaces

Oliver Ochs[1,2], Natalia Martsinovich[3], Wolfgang M. Heckl[1,2], and Markus Lackinger[1,2,]*

[1] Department of Physics, Technische Universität München, James-Franck-Str. 1, 85748
Garching, Germany

[2] Deutsches Museum, Museumsinsel 1, 80538 Munich, Germany

[3] Department of Chemistry, University of Sheffield, Sheffield S3 7HF, UK;

Materials and Methods

STM experiments

   STM experiments were conducted with the I-STM operated by a commercial SPM 100 control unit (RHK).[1] Sample temperatures (i.e. imaging temperatures) were varied between room temperature and ~70 °C, and held constant with a Eurotherm 2416 temperature controller. STM images were acquired using tunneling voltages between +0.25 V and +0.60 V (at the tip) and setpoint currents around ~50 pA. Mechanically cut Pt/Ir (90/10) wires used as STM tips without any further insulation, but were conditioned by short voltage pulses during the experiments. 2,6-naphthalenedicarboxylic acid (NDA, Sigma Aldrich, 99% pure) and nonanoic acid (9A, TCI chemicals, 98 % pure) were both used as received. For all desorption experiments NDA in 9A solutions were used with similar concentration of 0.11 mmol L^{-1}. These were obtained by diluting a saturated stock solution, and checked by UV-vis absorption spectroscopy. Freshly cleaved highly oriented pyrolytic graphite (grade ZYB, Optigraph GmbH) was used as substrate. For variable-temperature experiments the I-STM was filled with ~10 mL of solution, resulting in complete immersion of the sample.

Coverage measurements

   Molecular coverages were always evaluated the same way from a set of 25 large scale STM images (350 × 350 nm²) covering a total surface area of ~3.5 μm². Overlap between neighboring images was excluded by leaving a gap of at least 50 nm. Standard deviations were used as vertical error bars (see Figure S8). The origin of the time axis was defined as the time when the target temperature was reached after initial heating periods of ~30 min. The measurement halftime was used as time coordinate, and the (invisibly small) horizontal error bars correspond to the duration of ~90 min required for each measurement.

Dissolution enthalpy measurement

   To determine the dissolution enthalpy of NDA in 9A, a reservoir containing a relatively large amount of ~18 mL solution was heated to the target temperature. Saturation was ensured by the presence of a sediment. After the targeted measurement temperature was reached, the stock solution was stirred for ~2 h and allowed to settle and equilibrate for at least 20 h. For the actual measurement a small amount of the saturated solution was pipetted from the reservoir into the cuvette (1 mm optical path length, 110-QX macro-cuvette from Hellma Analytics) that was heated to the same temperature as the reservoir by Peltier elements.[2] Spectra were acquired with a USB4000 UV-vis spectrometer using a UV-vis-NIR light source (both Ocean Optics). Spectra of pure solvent from the same batch and heated to the same temperature served as reference. Measurements were performed for temperatures between 30.0 °C and 55.5 °C with increments of 2.5 °C. Measurement temperatures were varied non-monotonously to avoid and recognize kinetic effects.

Sublimation enthalpy measurement

The NDA sublimation enthalpy was determined by measuring the temperature dependence of effusion rates as proxy for saturated vapour pressure.[2] These were measured using a home-built Knudsen cell[3] and a water-cooled CNT06IG quartz crystal microbalance (Colnatex), operated by a Q-pod quartz crystal monitor (Inficon) in high vacuum.

Computational method

Molecular mechanics (MM) calculations were performed using the Tinker software[4] with the MM3 force field.[5-7] Modified force-field parameters were used for the cyclic O···H-O $R_2^2(8)$ hydrogen bonds in carboxylic acid dimers as previously proposed[8] to yield a binding energy of 66.9 kJ mol^{-1} in good agreement with experimental results[9] and both Density-Functional-Theory (DFT) and higher-level calculations.[10] For comparison, we also calculated NDA adsorption energies on graphite with DFT using previously optimized parameters.[11] The excellent agreement between DFT (-94.8 kJ mol^{-1}) and MM (-93.1 kJ mol^{-1}) derived NDA adsorption energies indicates high accuracy and appropriateness of MM calculations for aromatic carboxylic acids on graphite.

Lattice parameters of the NDA monolayer were optimized by systematically scanning through a range of values for the lattice vectors a, b, and the angle γ between them to find the minimum-energy structure, similar to a previously described procedure.[2, 12] Lattice parameters of NDA bulk crystals were optimized in a similar manner, by treating the 3D bulk structure as a stack of 2D layers. For these layers the previously optimized monolayer lattice parameters were used, while the lattice parameters c and the angles α and β were systematically varied to find the minimum-energy structure, similar to the procedure for the monolayers.[2]

Finite NDA islands of three sizes were considered: 3 × 3, 4 × 4 and 5 × 5 molecules. Binding energies were calculated in all non-equivalent positions as energy differences upon removing a single NDA molecule. In all calculations, i.e. monolayer, islands and bulk crystal, the z coordinates of all atoms were fixed to constrain the molecules the same plane, while the in-plane coordinates x and y were optimized.

Adsorption of both a single NDA molecule and a 5 × 5 NDA island on graphite were also calculated using MM. The graphite surface was modelled using extended hydrogen-terminated graphene sheets, comprised of 20 × 20 primitive hexagonal graphene unit cells (2 carbon atoms per unit cell, i.e. in total 800 C and 80 H atoms) for adsorption of a single NDA molecule and of 24 × 22 non-primitive rectangular graphene unit cells (4 carbon atoms per unit cell, i.e. in total 2112 C and 140 H atoms) for adsorption of the 5 × 5 NDA island. The extended graphene sheets were large enough to ensure that the adsorbed molecules were at least 10 Å away from the edges. Atomic positions within the graphene sheets were fixed, while the adsorbed NDA molecules were fully optimized. Positions and orientations of both the single adsorbed NDA molecule and the NDA island were investigated systematically by rotating the adsorbate through 120° (60° for the NDA island) in steps of 10° and translating each orientation of the adsorbate on a grid

covering the whole graphene unit cell in steps of 0.1 Å, similar to a previously reported procedure.[2]

Very small variations of NDA adsorption energies were observed depending on the position and orientation of the molecules: ≤ 0.95 kJ mol^{-1} variation for the single NDA molecule and ≤ 0.04 kJ mol^{-1} per one NDA molecule for the 5×5 island. Note that in the island the NDA molecules occupy a range of different adsorption sites because of the incommensurability of the NDA monolayer with the underlying graphene. These results shows that the variation in adsorption sites has very little effect on the substrate contribution to NDA desorption energies.

To estimate the wetting enthalpy, we used MM to calculate adsorption energies of single 9A solvent molecules on either the NDA monolayer or bare graphite. Thereby, we assume that the intermolecular contributions to wetting are essentially similar for both cases. On graphite, 9A adsorption energies are almost constant for various adsorption sites with a modest variation between (-69.7 ... -67.9) kJ mol^{-1}. We use a graphene unit cell averaged value of -68.6 kJ mol^{-1}. In contrast, 9A adsorption energies are as expected smaller on the NDA monolayer, and also exhibit larger site variations between (-67.5 ... -42.2) kJ mol^{-1}. We use a NDA unit cell averaged value of -49.1 kJ mol^{-1}. This results in a wetting enthalpy $\Delta H_{wet}(9A) = -19.5 \ kJ \ mol^{-1}$ for desorbing one 9A molecule from the NDA monolayer and re-adsorbing it on graphite. To derive an estimate for the wetting enthalpy $\Delta H_{wet}(NDA)$ per one NDA molecule, we renormalize $\Delta H_{wet}(9A)$:

$$\Delta H_{wet}(NDA) = \Delta H_{wet}(9A) \cdot \frac{A_{NDA}}{A_{9A}} = -19.5 \ kJ \ mol^{-1} \cdot \frac{0.712 \ nm^2}{0.679 \ nm^2} = -20.4 \ kJ \ mol^{-1}$$

A_{NDA} and A_{9A} correspond to the surface areas occupied by a single NDA and 9A molecule, respectively. Therefore, we used the area per molecule in ordered monolayers as obtained from the STM derived unit cell for NDA and literature reported unit cells for 9A.[13]
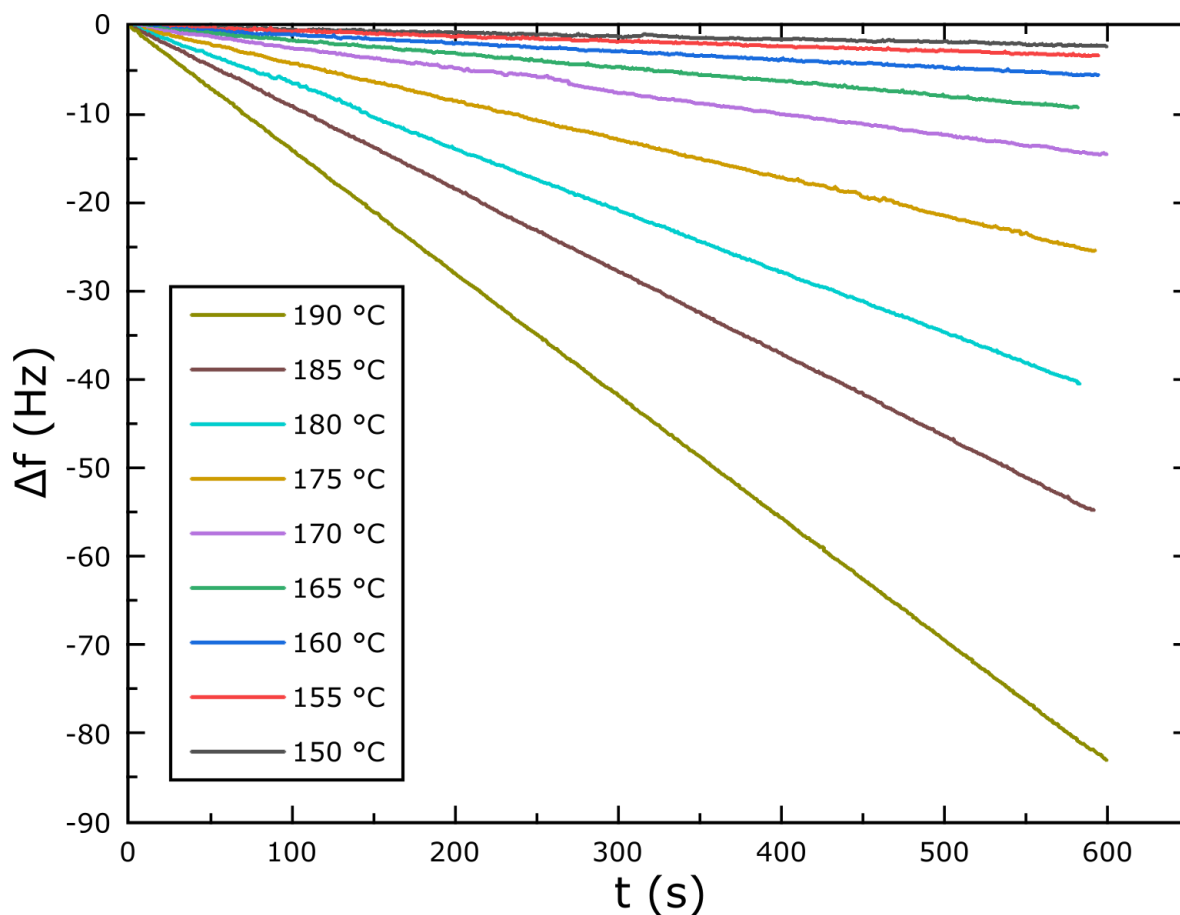
**Figure S1.** Effusion rate measurements of NDA with a Quartz Crystal Microbalance (QCMB). The graph shows resonant frequency shifts Δf versus time t traces, acquired for crucible temperatures of a Knudsen cell as indicated. The slopes of the respective traces were determined by fitting with straight lines, and correspond to the effusion rates used for the Van't Hoff plot shown in Figure S2.
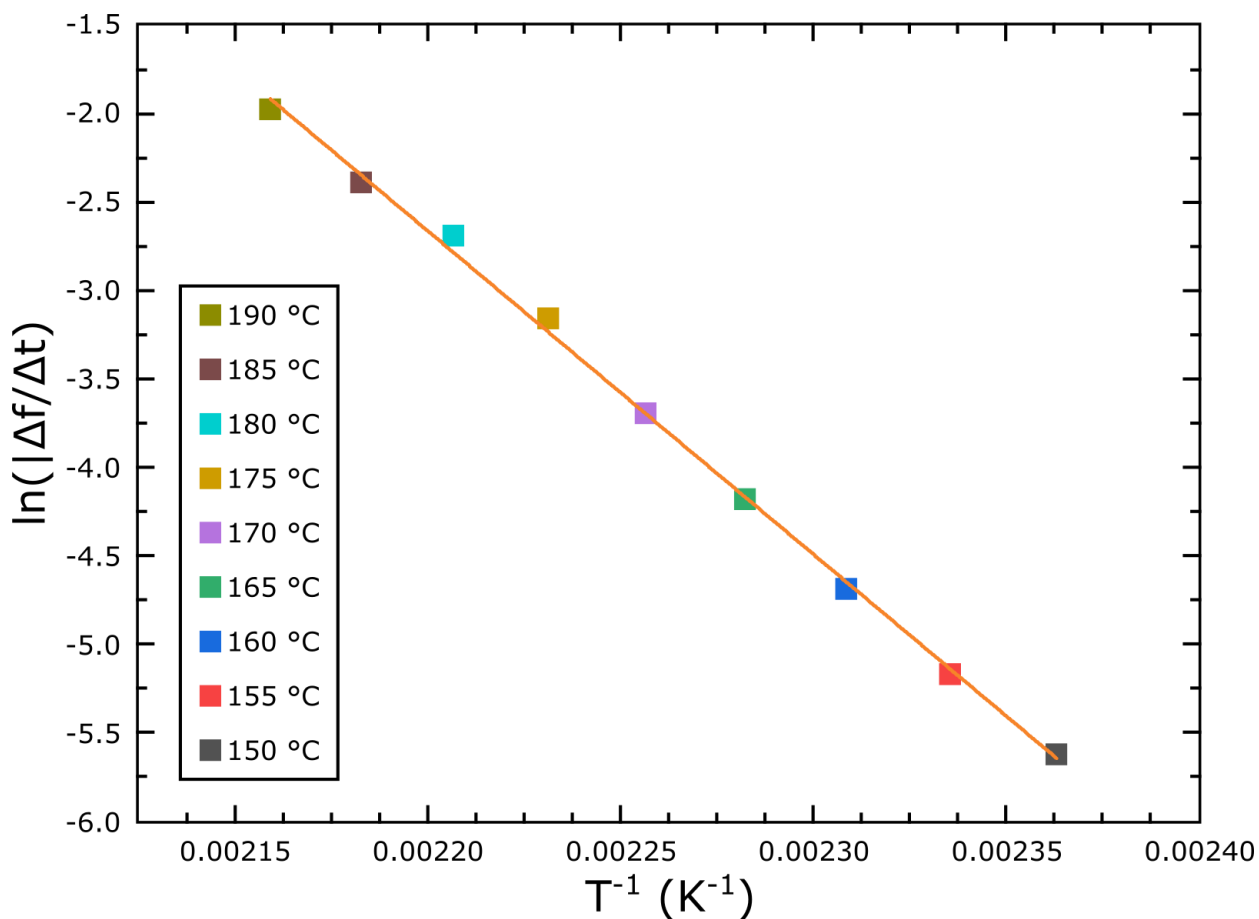
Figure S2. Van't Hoff plot of the NDA effusion rates (squares) extracted from the traces shown in Figure S1. The straight solid line represents a linear fit, and its slope corresponds to a NDA sublimation enthalpy of $\Delta H_{sub} = 152$ kJ mol^{-1}. The excellent agreement between data points and fit indicates a constant, i.e. temperature independent, sublimation enthalpy and the absence of chemical changes of NDA during the sublimation.
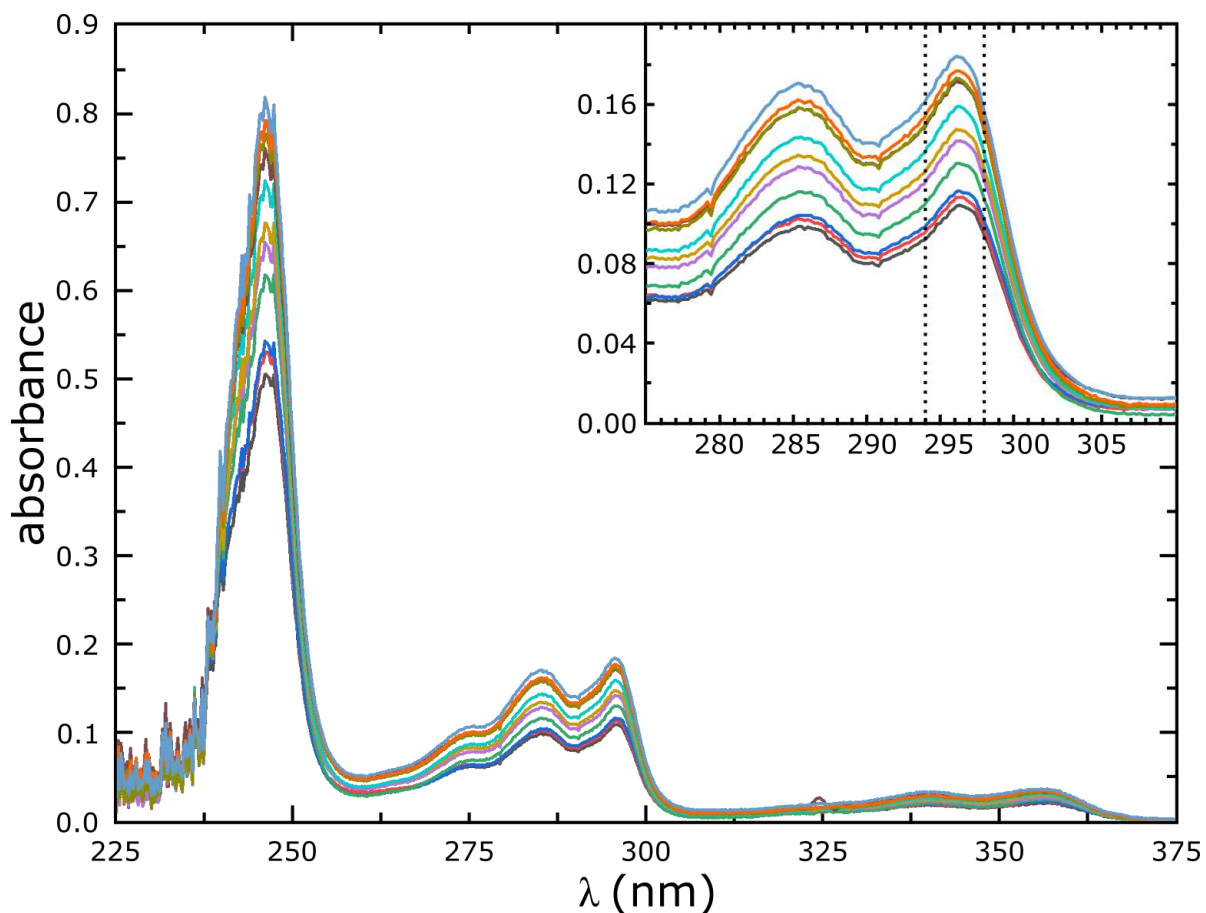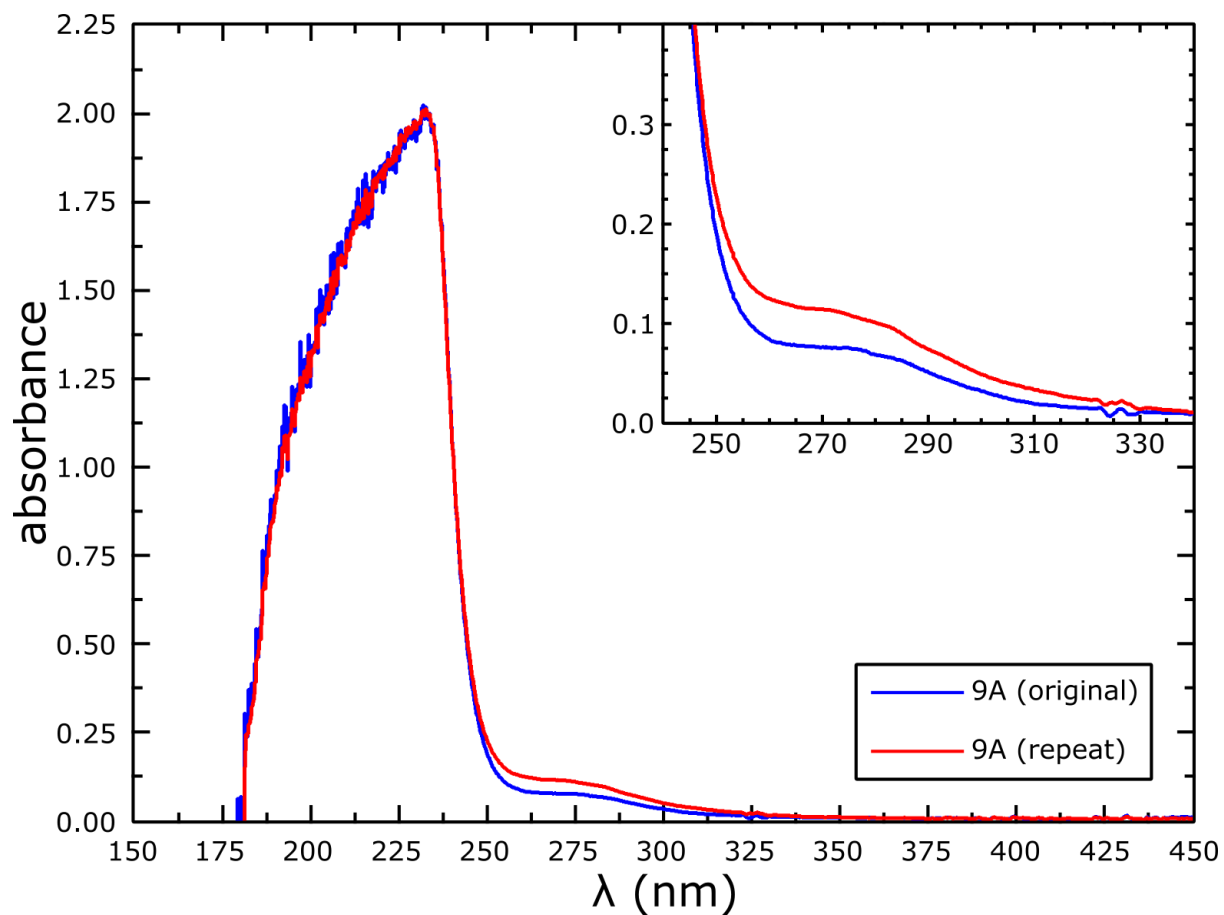
Figure S3. UV-vis absorption spectra of saturated NDA in 9A solutions acquired for temperatures between 30.0 °C (grey curve at the bottom) and 55.0 °C with temperature increments of 2.5 °C. The increasing absorbance (i.e. concentration) for increasing temperature indicates an endothermic dissolution. Integrated absorbances (in a wavelength range of $(294…298)$ nm, see insert) were used for the Van't Hoff plot shown in Figure S4. In this spectral range, the absorbances were reasonably low to yield reliable values and no peak shifts occurred as illustrated in the insert.
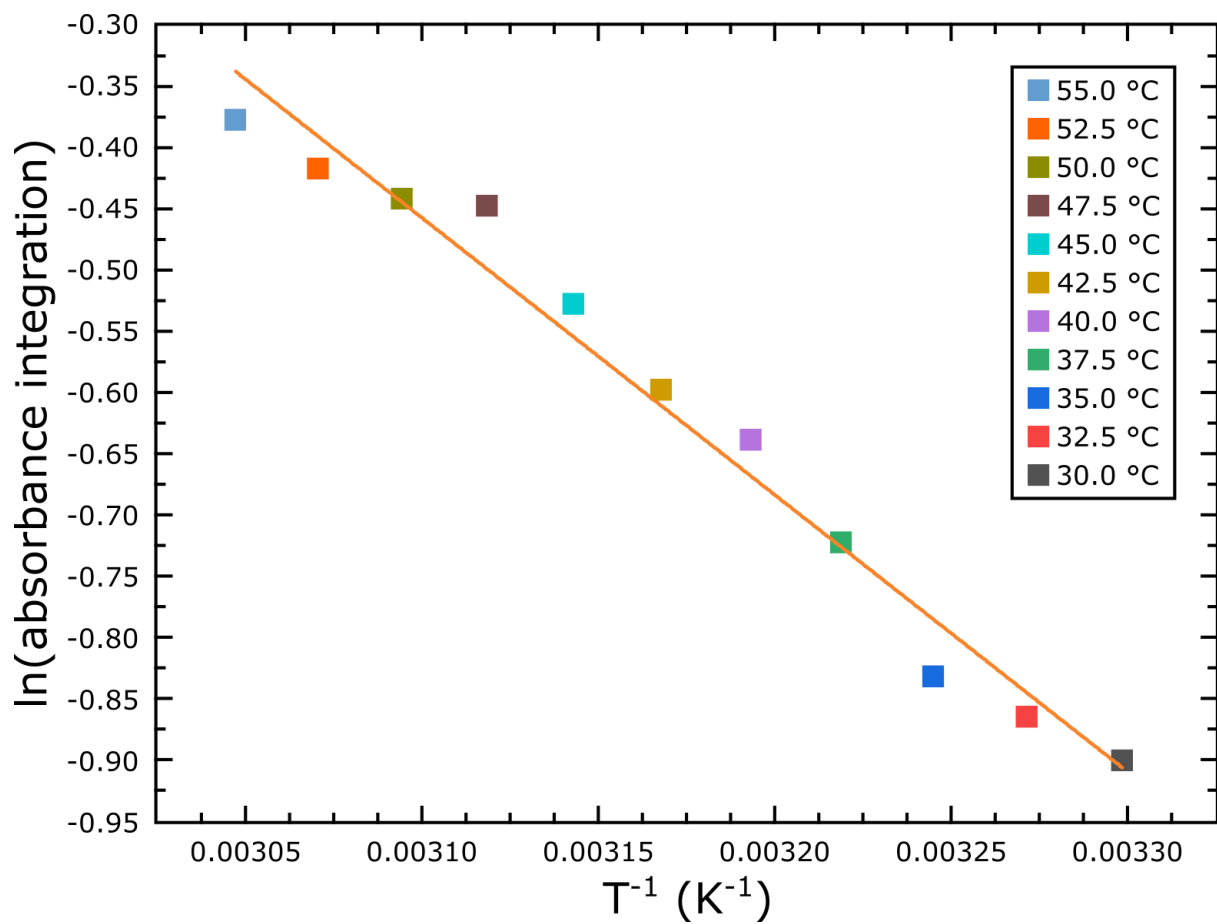
Figure S4. Van't Hoff plot of integrated absorbances of saturated NDA in 9A solutions (cf. Figure S3). The solid line represents a linear fit, and its slope corresponds to a NDA dissolution enthalpy of $\Delta H_{diss} = +18.8$ kJ mol^{-1}.
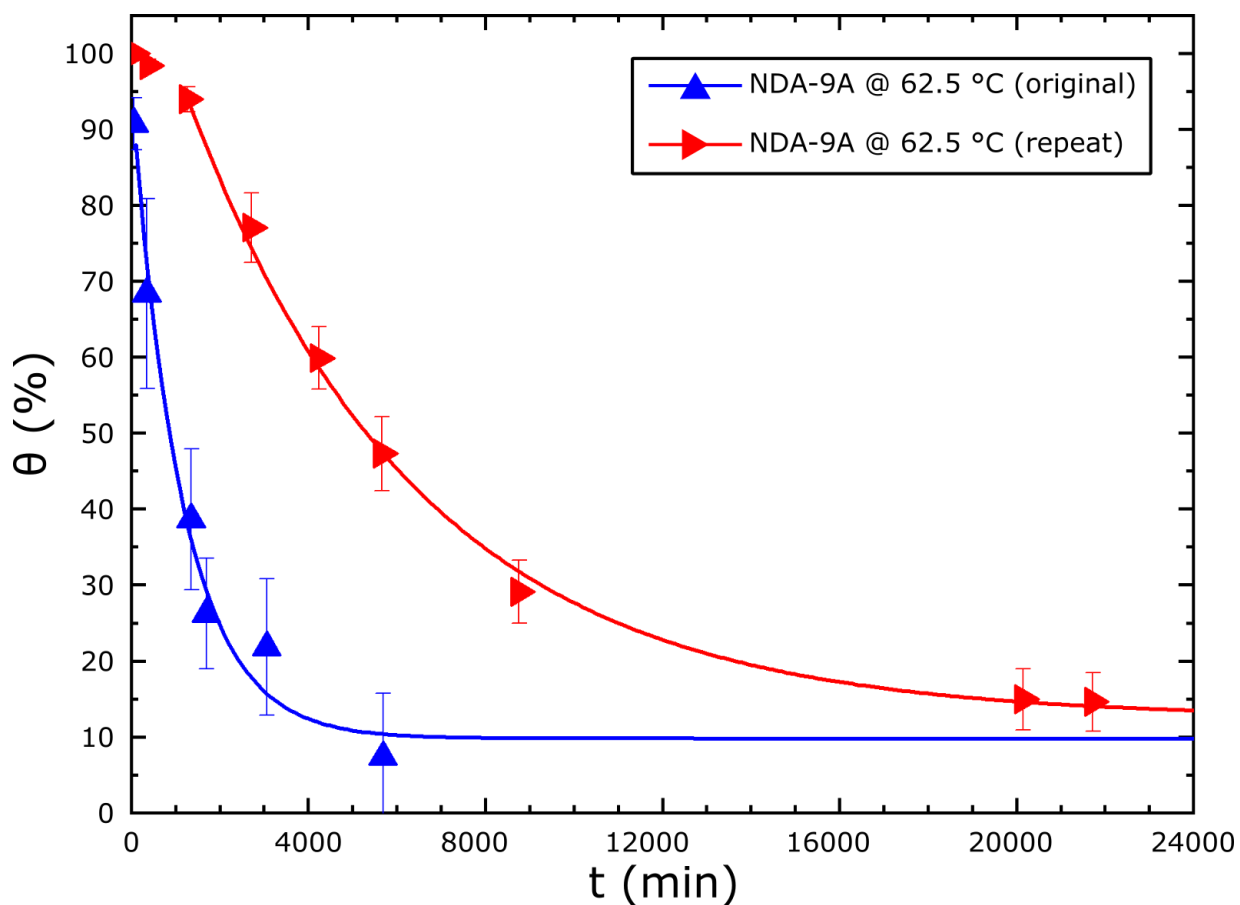
Figure S5. Desorption traces of NDA monolayers acquired at the 9A-graphite interface for the same temperature of 62.5 °C. The blue curve shows the same data as in the manuscript (Figure 2a), whereas the red curve presents data from a repeat experiment using 9A solvent from a different batch. Vertical error bars correspond to standard deviations, (invisibly small) horizontal error bars reflect the measurement duration. Solid lines represent fits with single exponential decays to an asymptotically reached final coverage resulting in $k = (8.7 \pm 1.49)\ 10^{-4}\ s^{-1}$ and $\theta_\infty = 9.8\ \%\ (\pm 4.52\ \%)$ for the original, and $k = (1.9 \pm 0.12)\ 10^{-4}\ s^{-1}$ and $\theta_\infty = 12.42\ \%\ (\pm 1.63\ \%)$ for the repeat experiment. Stated errors correspond to fitting uncertainties.

**Figure S6.** UV-vis absorption spectra of the pure 9A solvents used for the desorption traces shown in Figure S5. While the strong absorbance below 250 nm arises from the carboxylic acid groups, distinct differences in the spectral range (250…330) *nm* indicate both notable batch-to-batch variations and a less pure state of the solvent in the repeat experiment. The chemical origin of these variations, remains presently unclear.
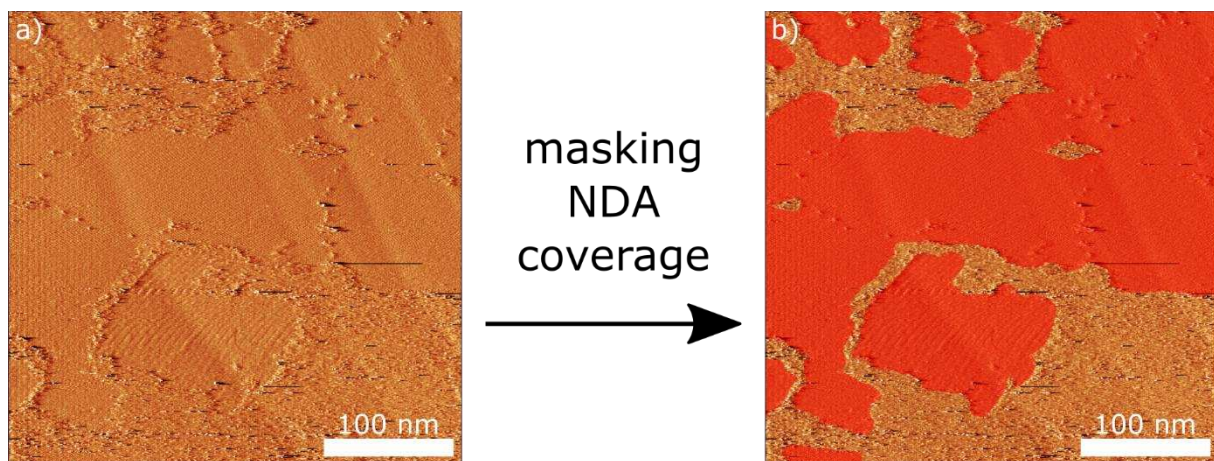
Figure S7. Example illustrating how molecular coverages were determined from individual STM images. (a) Original large scale (350 nm) STM image (current image, tunneling parameters: 0.59 V, 49.5 pA); Even though molecular details of the NDA domains cannot be inferred anymore at this magnification, it was always possible to unambiguously distinguish NDA domains from the uncovered graphite surface. (b) Processed image with NDA domains masked in red; Therefore a feature of the image processing software Gwyddion was used.[14] The ratio of the area marked in red to the total area of the image corresponds to the molecular coverage, i.e. ~64 % for the example here. For each coverage data point 25 of these large scale STM images were evaluated, Figure S8 shows a full series.
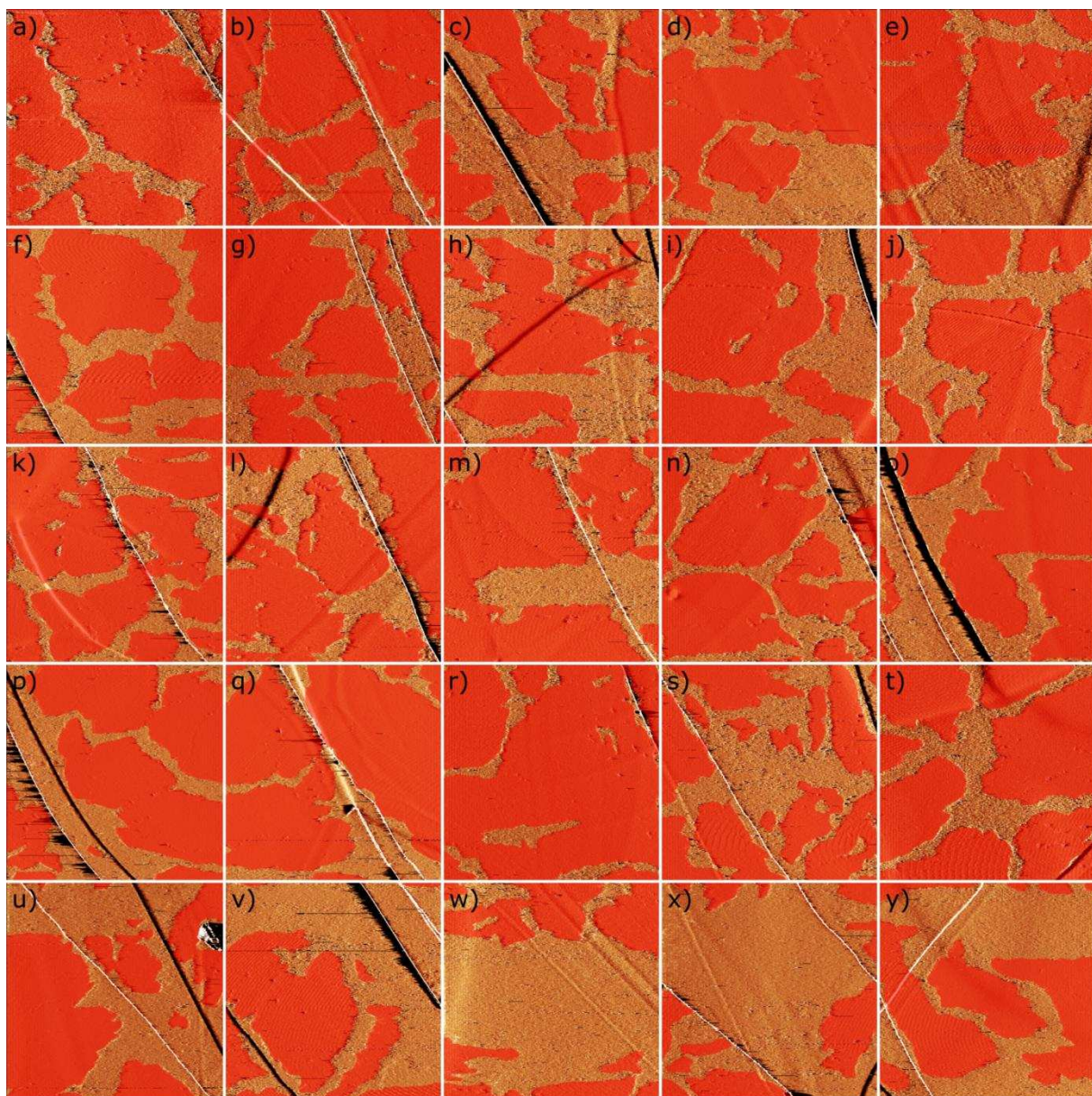
Figure S8. Complete series of 25 large scale STM images (350 × 350 nm², tunneling parameters: 0.59 V, ~50 pA) evaluated to determine a statistically significant coverage value. These images were acquired at 57.5 °C in ~77 min. of measurement time and were masked as described in Figure S7. Overlap between adjacent images was avoided by leaving a gap of at least 50 nm. Depending on the local topography (e.g. step edges) either forward or backward current images were used whichever provided more clear information.
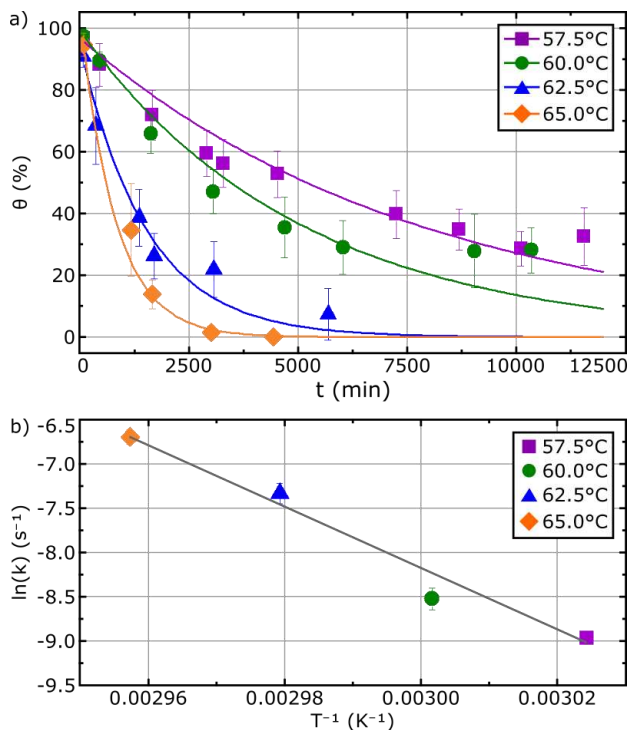
**Figure S9.** Summarized results of kinetic measurements on NDA monolayer desorption (same data set as in Fig. 2a of the main manuscript); **(a)** Molecular coverage θ vs. time t traces measured by STM at fixed temperatures (purple squares: 57.5 °C; green dots: 60.0 °C; blue triangles: 62.5 °C; orange diamonds: 65.0°C); Vertical error bars correspond to standard deviations, and (invisibly small) horizontal error bars reflect the measurement duration of ~90 min. Solid lines represent fits with single exponential decays to zero (i.e. $\theta_\infty = 0$ % set for all desorption traces) (cf. Table S1 for a summary of the fitting results). **(b)** Arrhenius plot of the rate constants. The solid line represents a linear fit, with a slope corresponding to an activation energy of +289 kJ mol^{-1}. Fitting uncertainties account for vertical error bars. Fitting the desorption traces with single exponential decays, i.e. neglecting finite partial coverages, results in a significantly higher activation barrier.

Table S1. Rate constants k as obtained from fitting desorption traces in Fig. S9a acquired at temperatures T with single exponential decays to zero; fitting uncertainties are stated in parenthesis;

| T (°C)	k (10^{-4} min^{-1})
57.5	1.27 (±0.09)
60.0	1.98 (±0.24)
62.5	6.56 (±0.74)
65.0	12.4 (±1.04)
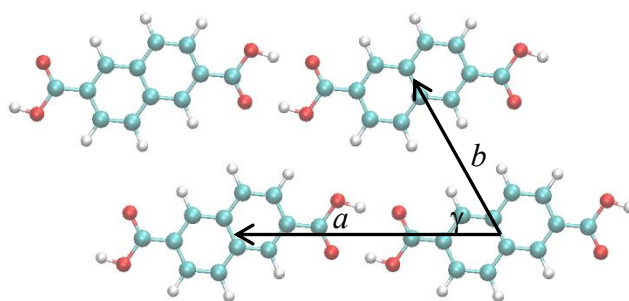
Figure S10. NDA monolayer structure as obtained by MM calculations. The optimised lattice parameters are: a = 1.15 nm (corresponding to the repeat distance along the H-bonded chains), b = 0.74 nm, γ = 60.0°.
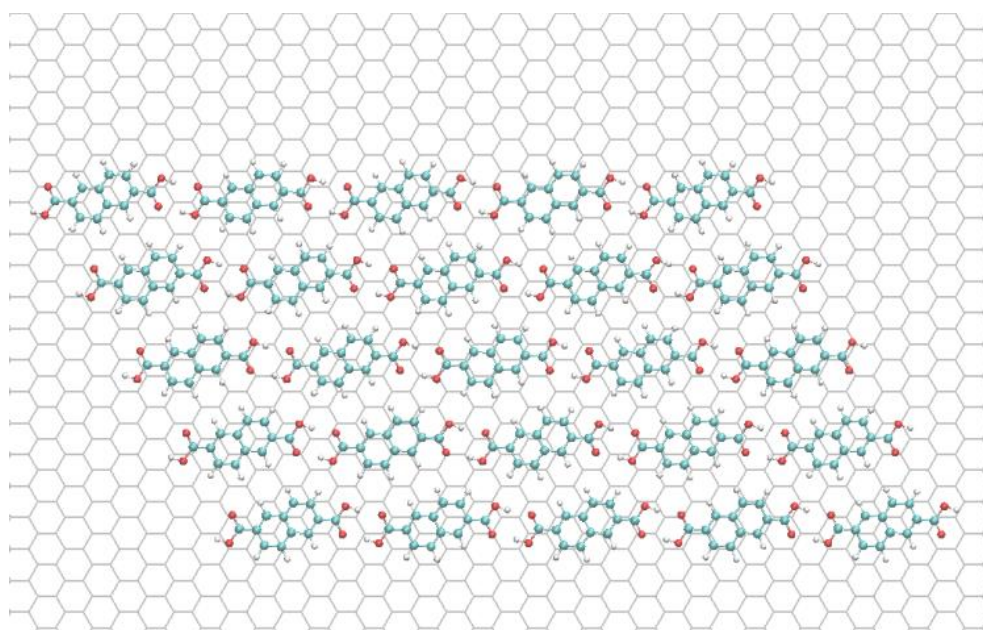
Figure S11. MM optimized finite island comprised of 5×5 NDA molecules on graphene (not fully shown here). This structure corresponds to the energy minimum for all positions and orientations probed. Yet, the energy variations were relatively small, also because of averaging over the non-equivalent NDA adsorption sites in this incommensurate structure.
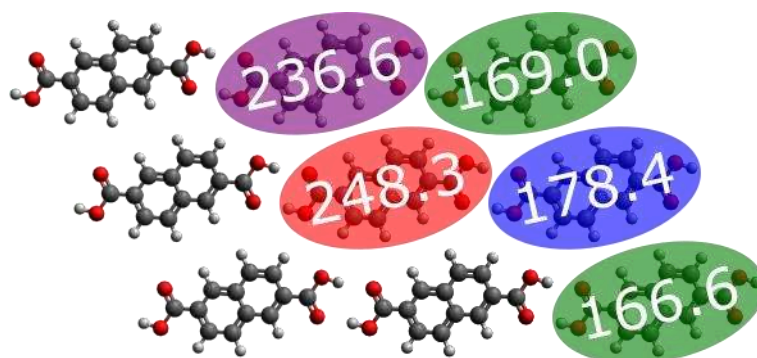
Figure S12. MM derived desorption energies of NDA molecules (in kJ mol^{-1}) from a finite island comprised of 3×3 NDA molecules. Calculations were conducted on graphite(0001) (not shown for clarity). Desorption energies for edge molecules are similar to results obtained on a larger 5×5 island (see Figure 3 main manuscript), indicating that desorption energies are only diminished for molecules directly at the domain edge.
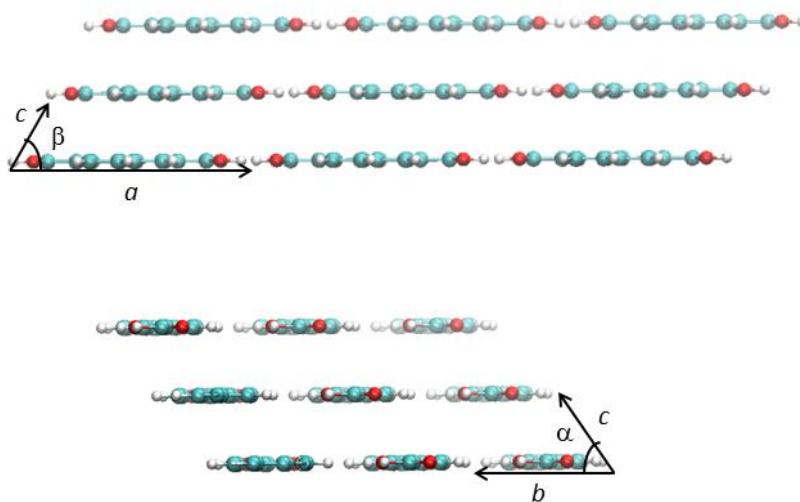
Figure S13. NDA bulk structure as obtained by MM calculations. The optimised lattice parameters are: a = 1.15 nm, b = 0.74 nm, c = 0.45 nm, α = 74.7°, β = 63.9°, γ = 60.0°.

References

(1)   Ochs, O.; Heckl, W. M.; Lackinger, M., Immersion-scanning-tunneling-microscope for long-term variable-temperature experiments at liquid-solid interfaces. *Rev. Sci. Instrum.* **2018,** *89* (5), 053707.

(2)   Song, W.; Martsinovich, N.; Heckl, W. M.; Lackinger, M., Born–Haber Cycle for Monolayer Self-Assembly at the Liquid–Solid Interface: Assessing the Enthalpic Driving Force. *J. Am. Chem. Soc.* **2013,** *135* (39), 14854-14862.

(3)   Gutzler, R.; Heckl, W. M.; Lackinger, M., Combination of a Knudsen effusion cell with a quartz crystal microbalance: In situ measurement of molecular evaporation rates with a fully functional deposition source. *Rev. Sci. Instrum.* **2010,** *81* (1), 015108.

(4)   Ponder, J. W.; Richards, F. M., An efficient newton-like method for molecular mechanics energy minimization of large molecules. *J. Comput. Chem.* **1987,** *8* (7), 1016-1024.

(5)   Allinger, N. L.; Yuh, Y. H.; Lii, J. H., Molecular mechanics. The MM3 force field for hydrocarbons. 1. *J. Am. Chem. Soc.* **1989,** *111* (23), 8551-8566.

(6)   Lii, J.-H.; Allinger, N. L., Directional hydrogen bonding in the MM3 force field. I. *J. Phys. Org. Chem.* **1994,** *7* (11), 591-609.

(7)   Lii, J.-H.; Allinger, N. L., Directional hydrogen bonding in the MM3 force field: II. *J. Comput. Chem.* **1998,** *19* (9), 1001-1016.

(8)   Martsinovich, N.; Troisi, A., Modeling the Self-Assembly of Benzenedicarboxylic Acids Using Monte Carlo and Molecular Dynamics Simulations. *J. Phys. Chem. C* **2010,** *114* (10), 4376-4388.

(9)   Allen, G.; Watkinson, J. G.; Webb, K. H., An infra-red study of the association of benzoic acid in the vapour phase, and in dilute solution in non-polar solvents. *Spectrochim. Acta* **1966,** *22* (5), 807-814.

(10)   Colominas, C.; Teixidó, J.; Cemelí, J.; Luque, F. J.; Orozco, M., Dimerization of Carboxylic Acids: Reliability of Theoretical Calculations and the Effect of Solvent. *J. Phys. Chem. B* **1998,** *102* (12), 2269-2276.

(11)   Ochs, O.; Hocke, M.; Spitzer, S.; Heckl, W. M.; Martsinovich, N.; Lackinger, M., Origin of Solvent-Induced Polymorphism in Self-Assembly of Trimesic Acid Monolayers at Solid–Liquid Interfaces. *Chem. Mater.* **2020,** *32* (12), 5057-5065.

(12)   Della Pia, A.; Luo, D.; Blackwell, R.; Costantini, G.; Martsinovich, N., Molecular self-assembly of substituted terephthalic acids at the liquid/solid interface: investigating the effect of solvent. *Faraday Discuss.* **2017,** *204* (0), 191-213.

(13)   Bickerstaffe, A. K.; Cheah, N. P.; Clarke, S. M.; Parker, J. E.; Perdigon, A.; Messe, L.; Inaba, A., The Crystalline Structures of Carboxylic Acid Monolayers Adsorbed on Graphite. *J. Phys. Chem. B* **2006,** *110* (11), 5570-5575.

(14)   Nečas, D.; Klapetek, P., Gwyddion: an open-source software for SPM data analysis. *CEJPh* **2012,** *10* (1), 181-188.